ORIGINAL RESEARCH

A holistic human activity recognition optimisation using AI techniques

Zhenghui Li[1] | **Yushi Liu**[1] | **Bo Liu**[1] | **Julien Le Kernec**[1] | **Shufan Yang**[2]

[1]School of Engineering, University of Glasgow, Glasgow, UK

[2]School of Computing, Edinburgh Napier University, Edinburgh, UK

Correspondence

Julien Le Kernec.
Email: julien.lekernec@glasgow.ac.uk

Funding information

Engineering and Physical Sciences Research Council, Grant/Award Number: EP/T021020/1

Abstract

Building on previous radar-based human activity recognition (HAR), we expand the micro-Doppler signature to 6 domains and exploit each domain with a set of handcrafted features derived from the literature and our patents. An adaptive thresholding method to isolate the region of interest is employed, which is then applied in other domains. To reduce the computational burden and accelerate the convergence to an optimal solution for classification accuracy, a holistic approach to HAR optimisation is proposed using a surrogate model-assisted differential evolutionary algorithm (SADEA-I) to jointly optimise signal processing, adaptive thresholding and classification parameters for HAR. Two distinct classification models are evaluated with holistic optimisation: SADEA-I with support vector machine classifiers (SVM) and SADEA-I with AlexNet. They achieve an accuracy of 89.41% and 93.54%, respectively. This is an improvement of ~11.3% for SVM and ~2.7% for AlexNet when compared to the performance without SADEA-I. The effectiveness of our holistic approach is validated using the University of Glasgow human radar signatures dataset. This proof of concept is significant for dimensionality reduction and computational efficiency when facing a multiplication of radar representation domains/feature spaces and transmitting/receiving channels that could be individually tuned in modern radar systems.

KEYWORDS

evolutionary computation, pattern classification, radar, radar signal processing

1 | INTRODUCTION

Indoor human activity recognition (HAR) has grown significantly in recent years and gained substantial interest in fields, such as assisted living, smart homes and security [1]. Several different sensing technologies, including wearable sensors, video-based systems, and radio frequency sensors [2], have been presented. Wearable sensors, which require to be worn constantly to be effective, can cause discomfort and have high false alarm [3]. Video-based systems, such as camera, can lead to privacy invasion and disputes over image rights. It is also vulnerable to lighting conditions [1]. Radio frequency sensing, especially radar, can effectively complement conventional technologies. Its contactless capabilities eliminate the need for end-users to wear, carry, or interact with any additional device,

which can increase user acceptance and compliance [4]. Furthermore, the absence of plain images or videos to be recorded can help address potential privacy concerns. In assisted living, radar sensors are being developed commercially by companies, such as Vayyar, Xandar Kardian. Furthermore, it is actively researched in academia [4, 5].

The traditional radar-based HAR mainly focuses on the Micro-Doppler signature (MDS). The MDS allows the investigation of limb motion relative to the trunk, which constitutes the main Doppler components. It is widely utilised in radar-based HAR since it provides salient features to distinguish activities [6]. Considerable research in HAR focuses on MDS, that is, the amplitude of MDS, also known as the spectrogram, using both hand-crafted features and deep learning models [1, 4, 5, 7].

In addition to the amplitude of MDS, several radar data domains and techniques are available for HAR, such as range-time (RT), range-Doppler, MDS, Radon, Cepstrogram, Cyclostationarity [8], composite domains [9] and point clouds [10]. This variety of domains multiplies the data representations further by considering the complex nature of the radar matrices produced by signal processing giving rise to amplitude, phase, real, and imaginary data. Meanwhile, various pre-processing parameters, such as different sizes of short-time Fourier Transforms on the range bins in slow time, different windowing functions, different padding factors, etc., were also proposed to classify different activities [11, 12]. Two papers [13, 14] based on the TI MIMO radar use point clouds for real-time classification with a robot operating system (ROS) framework. In [13], the authors extract point clouds of targets using a constant false alarm rate filter and then generate the micro-Doppler signatures on a host computer before classification with a convolutional neural network (CNN) achieving over 90% accuracy with 6 classes. In [14], the authors use an ROS framework in the 3D point clouds of 5 activities directly for classification with a CNN to extract features for each frame and a bi-LSTM neural network across 60 frames to analyse the temporal links between frames forward and backward achieving 90.47%.

Table 1 lists a number of other papers using different datasets, different signal processing parameters and classification algorithms that were tuned manually. The obtained performances are good, but they could be better. Identifying the optimal radar data domains and their pre-processing parameters optimisation for a particular classification task becomes an intractable problem for parametric sweeping as well as exploring the most suitable combination of salient features. Expanding on our previous results [26–28], we propose a patented adaptive thresholding approach to extract the region of interest (ROI) in multi-domain MDS with new hand-crafted features. This method is intended to delineate the ROI, that is, the targeted most relevant part of the MDS, also referred to as a 'mask'. Afterwards, the 'mask' is applied to other domains, such as a phase to emphasise the ROI in those domains, hence generating several new representations.

Optimising the pre-processing parameters for thresholding, MDS generation and the selection of the best representations to maximise classification accuracy is a challenge for parametric sweeping, since it is intractable for such problems with ever-expanding parameters to tune, which is computationally expensive and time-consuming. Furthermore, some off-the-shelf modern optimisation techniques, such as differential

TABLE 1 Human activity recognition (HAR) review of radar data domain usage and performances.

Ref	HW	Classification algorithm	# of classes	Radar data domain	Performance metrics	Best performance
[10]	FMCW MIMO	PointNet++, LSTM	8 (easy)	Cloud point	Accuracy	96.6% for easy set
			12 (complex)			95.1% for complex set
[15]	FMCW	SVM, KNN	6	Doppler-time maps, CVD	Accuracy	95.4% for HAR
[12]	FMCW MIMO	LSTM + CNN	7	Doppler-time maps	Precision, recall, F1-score, accuracy	Precision: 98%
						Recall: 98%
						F1-score: 98%
						Acc = 98.28%
[16]	FMCW	LSTM	2	Raw radar data, range maps	Accuracy	99.56%
[17]	FMCW	SAE	4	Doppler-time maps, range maps.	Accuracy	96.4%
[18]	FMCW MIMO	ANN	8	Doppler-time maps, range maps.	Accuracy	99.21%
[19]	FMCW	CNN	5	Doppler-time maps, range maps.	Accuracy	97.2%
[20]	FMCW	Bi-LSTM	6	Doppler-time maps	Accuracy	96%
[21]	FMCW	KNN	6	Doppler-time maps	Accuracy	95.5%
[22]	FMCW	CFFN (CNN + MLP)	6	Range-Doppler surface, phase	Accuracy	94%
[23]	FMCW	CNN (PointNet), LSTM	5	3D could point	Accuracy	90%
[24]	FMCW	MB-GAN	5	Doppler-time maps	Accuracy	89.83%
[24]	FMCW	CNN + LSTM	6	Range-Doppler maps	Accuracy	98.02%
[25]	FMCW	CNN + LSTM	6	Range-Doppler map	Accuracy	Accuracy: 96.2%
					Recall	Recall: 96%
[13]	FMCW MIMO	CNN	6	Doppler time maps	Accuracy	90.68%
[14]	FMCW MIMO	CNN + Bi-LSTM	5	Cloud points	Accuracy	90.47%

Abbreviations: ANN, artificial neural network; CFFN, complex field-based fusion network; CNN, convolutional neural network; HW, hardware; KNN, K nearest neighbour; LSTM, long short term memory; MLP, multilayer perceptron; SAE, stacked auto-encoder.

evolution (DE) [29] and particle swarm optimisation [30], are still too expensive to utilise in this case.

This paper investigates a holistic HAR optimisation using Surrogate Model-Assisted DE Algorithm (surrogate model-assisted differential evolutionary algorithm (SADEA-I)) [14, 26] in which the MDS domain is used as a proof of concept before expanding this technique to a wider range of parameters and other radar data domains to include the pre-processing, domain selection, feature selection, and machine learning/deep learning joint optimisation. The specific contributions and novelty, which distinguish this work from the current state of the art, are summarised here:

- This is the first proof-of-concept of the efficient self-tuning joint-optimisation of signal processing and machine learning parameters using an Evolutionary Algorithm (EA). This is a novel approach in HAR to optimise the classification accuracy automatically to find the global maximum performance in a fraction of the time required by an expert human operator. This is based on SADEA-I, as a machine learning-assisted EA, employed for the efficient joint optimisation of the signal pre-processing parameters and a combination of radar representations to minimise the classification error rate through an effective global search and performance predictions to reduce the computational load.
- A novel signal processing approach is proposed incorporating with our patented techniques and exploiting complex information. We introduce a radar-based HAR information processing method using adaptive thresholding that automatically produces ROI for human MDS yielding 6 different domains—Unfiltered MDS amplitude, Binary Mask, Masked phase, Masked unwrapped phase, Masked spectrogram (patent), Masked MDS complex matrix. To the best of our knowledge, phase domain has been marginally explored for radar-based HAR.

- Our approach is validated using both statistical learning based on extracted features and deep learning classifiers with vision-based algorithms. This serves to showcase the potential of this self-tuning joint-optimisation technique to enhance the performances of HAR architecture to obtain the best performances.

The goal is not to automatically reach the general maximum for HAR based on a set of tuning parameters, signal processing, and machine learning outperforming an expert operator. Note that this proof-of-concept may not be the best of all performances in the literature, but the global maximum for the given architecture, the EA is tuning. We combine both expert knowledge and artificial intelligence by setting an architecture for signal processing and classification as well as leveraging EA to efficiently self-tune the parameters jointly to optimise performances.

This paper is structured as follows: Section 2 describes the methods used in this investigation. Section 3 presents the result of optimisation, and Section 4 draws conclusions.

2 | METHODOLOGY

Figure 1 provides a depiction of the complete methodology employed in our algorithm. The process commences with the raw data undergoing signal processing via the SADEA algorithm, which assists in determining the parameters during the signal processing stage. This procedure consequently leads to the generation of varying radar representations with different signal processing methodologies.

Subsequently, these radar domains are channelled either towards a hand-crafted feature extraction algorithm or directly fed into neural networks for automatic feature extraction. The hand-crafted approach utilises expert knowledge in signal
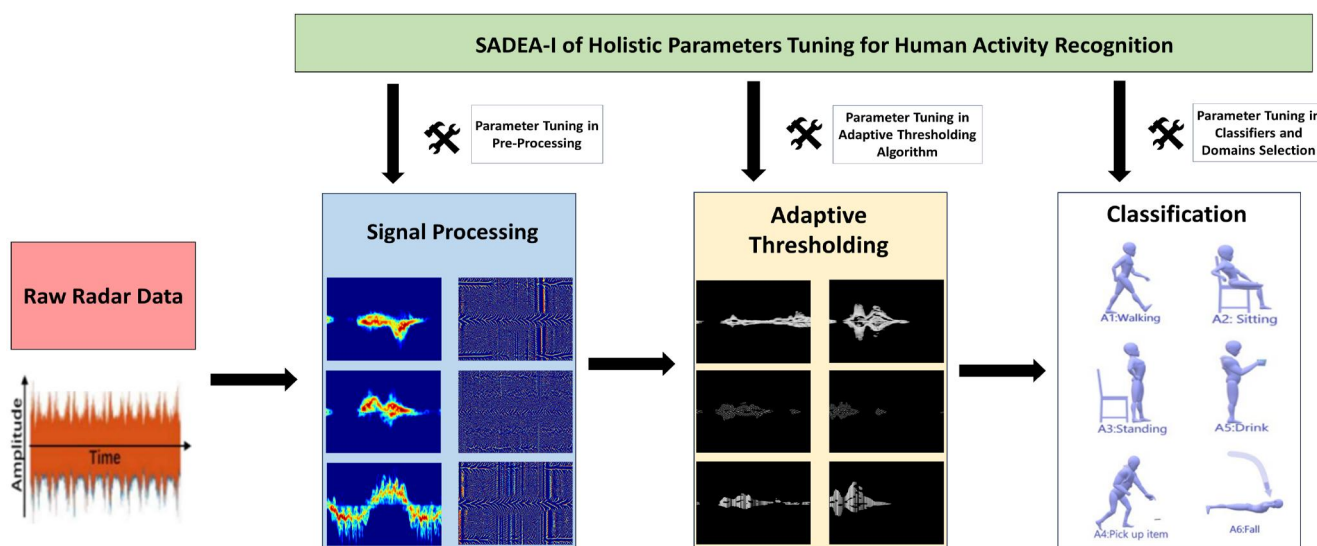

FIGURE 1 Holistic human activity recognition (HAR) Optimisation from signal processing to classification with surrogate model-assisted differential evolutionary algorithm (SADEA-I).

processing to extract characteristic features from the radar domains, whereas the neural network method allows for automated learning and extraction of relevant features from the raw data.

2.1 | Dataset

The experiments are conducted on the University of Glasgow Radar Signature dataset [31, 32]. A total of 1754 motion files were captured from 72 individuals aged 21–98 years old. Data acquisition was accomplished through a Frequency Modulated Continuous Wave radar system, functioning at a frequency of 5.8 GHz. This system showcased a swift pulse repetition period of 1 millisecond, a broad bandwidth of 400 MHz, and a capacity to record 128 complex samples per sweep. The radar was connected to a pair of Yagi antennas, employed for both the transmitting and receiving of signals, demonstrating an appreciable gain of approximately +17 dBi. This dataset is summarised in Table 2. Note that the dataset is not balanced as the older participants did not perform the 'fall' task for their safety. The activities were chosen to be challenging from the perspective of recognition in the context of assisted living. Activities 4 and 5 are particularly difficult to recognise from one another [5].

2.2 | Pre-processing

The radar raw data is converted into an RT map using a windowed Fast Fourier Transform. This window could be Hamming or Rectangular. After obtaining the RT map, the MDS is generated using a Short-Time Fourier Transform with a W s Hamming window and an F% overlapping factor on the RT map. The RT window, W and F are parameters tuned in the following steps.

Previously in [33], we found that varying the length of time of clip of MDS had an effect on the classification result. In this experiment, the radar data would be clipped into pieces with K s, and K is an optimisable parameter.

2.3 | Adaptive thresholding method

The proposed approach [26–28] can binarise the grayscale MDS image using a specific threshold T. This method

TABLE 2 Summary of the dataset.

No.	Activity description	Number of samples	Data length
A1	Walking back and forth	312	5s
A2	Sitting down on a chair	312	5s
A3	Standing up from a chair	311	5s
A4	Picking up an object	311	5s
A5	Drinking water	310	5s
A6	Fall	198	5s

adaptively focuses on the ROI by setting a threshold and then adjusting it depending on the data included in the window being analysed. The MDS amplitude image is first converted into grayscale. Suppose that the grayscale image S contains N pixels, and the value of each pixel is represented as $I(x, y)$, then the initial threshold μ could be expressed as Equation (1).

$$\mu = \frac{1}{N} \sum_{I(x,y) \in S} I(x, y) \qquad (1)$$

Based on the initial threshold value μ, the grayscale spectrogram image is divided into two portions: P_1 and P_2, where P_1 is the image region with a pixel value greater than μ and P_2 is the image area with a pixel value less than μ. Then, a new threshold T can be calculated as Equation (2).

$$T = \frac{1}{2} \left[\frac{1}{N_1} \sum_{I(x,y) \in p_1} I(x, y) + \frac{1}{N_2} \sum_{I(x,y) \in p_2} I(x, y) \right] \qquad (2)$$

where N_1 and N_2 are the number of pixels in part P_1 and part P_2, respectively.

Following the acquisition of both μ and T, their difference will be compared to a specific parameter: V. If the difference is greater than V, then T will be substituted by μ to segment the grayscale spectrogram image, and a new T will be determined using Equation (2). The procedure is repeatedly performed until the difference is less than V, thus maintaining as much ROI as possible. To investigate the impacts of the adaptive threshold, an additional offset T_e is added to the calculated threshold T to obtain the final value T_f (Equation (3)). Note that both V and T_e are parameters tuned at the optimisation stage.

$$T_f = T + T_e \qquad (3)$$

The grayscale spectrogram image is binarised by the T_f and the process can be phrased as in Equation (4).

$$b(x, y) = \begin{cases} 1, I(x, y) \geq T_f \\ 0, I(x, y) < T_f \end{cases} \qquad (4)$$

where $b(x, y)$ is the pixel value of the mask.

The binarised image, called 'mask', can be used for feature extraction. The mask can also be applied to the other MDS representations to acquire a 'masked' MDS domain as Equation (5).

$$M_{masked\ information} = M_{mask} \times M_{other\ domain} \qquad (5)$$

Figure 2 illustrates the domains used in this paper and the process of calculating the domains. They are subsequently named: Unfiltered MDS amplitude, Binary Mask, Masked phase, Masked unwrapped phase, Masked spectrogram (patent), Masked MDS complex matrix, and labelled as MDS domains 1–6, respectively.
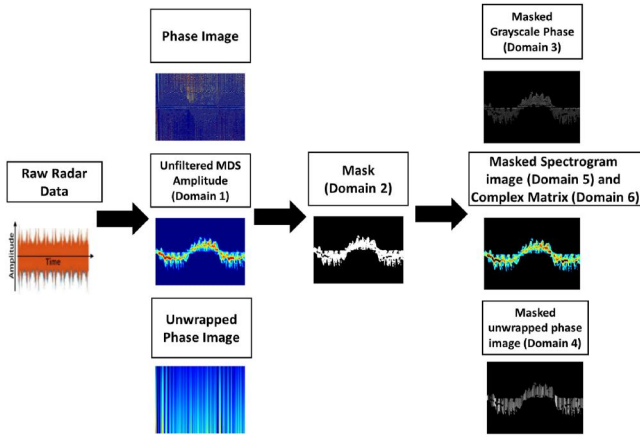
FIGURE 2 The process of obtaining micro-Doppler signature (MDS) domains.

2.4 | Features

User-specified features can portray the data in a salient manner, and it has been shown that it can outperform deep neural network feature extraction while reducing the computational load [34]. The features used in this paper are divided into two groups. Group 1, also referred to as 'patent features', comprising 68 in total, is applied to MDS domains 2–4. Two categories are considered: the properties of the ROI and the texture of the image. They are listed in Table 3 with the application domains. Note that despite being analytically defined, they vary from one MDS representation to the next. Group 2, also known as 'radar features', is used for Domain 1 and 6. This includes 22 features listed in Table 4 with their application domains.

The combination process of various representations is shown in Equations (6) and (7). y_N determines whether the $domainN$ ($N = 1, 2, 3, 4, 5, 6$) is included ($y_N = 1$) or excluded ($y_N = 0$) from the combination process where $\cap$ represents the concatenation of features from different domains.

$$F_{domainNy_N} = \begin{cases} F_{domainN}, y_N = 1 \\ \varnothing, y_N = 0 \end{cases} \quad (6)$$

$$F_{combination} = F_{domain1y_1} \cap F_{domain2y_2} \cap \ldots \cap F_{domain6y_6} \quad (7)$$

2.5 | Classification

Based on the features and combination process listed above, the classification models are trained using a machine learning model and a deep learning model, respectively, which are a quadratic kernel support vector machine classifiers (SVM) [7] and an AlexNet [35]. Support vector machine classifiers has been used in [34] outperforming deep learning and Alexnet is a light implementation of a deep network. These 2 classification methods were chosen to demonstrate that the SADEA algorithm can self-tune the signal processing and radar data domain

TABLE 3 Patent features and their applicable domains.

ROI features	Feature dimensions	Applicable domains
Perimeter of ROI	1×1	Domains 2, 3, 4 and 5
Area of ROI	1×1	
Centroid of ROI	1×2	
Eccentricity of ROI	1×1	
Orientation of ROI	1×1	
Major and minor axis length of ROI	1×2	
Textural features	**Feature dimensions**	
Local binary pattern of image	1×59	
Moment of image	1×1	
The number of total features	**68**	

Note: Bold values indicate the number of features.

TABLE 4 Spectrogram features and their applicable domains.

Radar features	Feature dimensions	Applicable domains
Entropy of spectrogram	1×1	Domain 1 and domain 6
Skewness of spectrogram	1×1	
Kurtosis of spectrogram	1×1	
Centroid of spectrogram (mean and variance)	1×2	
Bandwidth of spectrogram (mean and variance)	1×2	
Energy curve (mean and variance and trapezoidal numerical integration)	1×3	
Singular vector decomposition (mean and variance of the first three vectors of components)	1×12	
The number of total features	**22**	

Note: Bold values indicate the number of features.

selection with statistical learning and deep learning approaches and gauge performances against deep learning algorithms.

The machine learning operates efficiently with relatively fewer resources, thus our primary concern when selecting a model is its performance. The SVM model can achieve the best results in terms of our previous research. The option for AlexNet in our project was driven by its straightforward structure, facilitating easy understanding and implementation. The performance is also robust, and its computational efficiency attributed to its relatively smaller size. These features make it as an ideal deep learning choice for us, that is, a resource-constrained environments.

For machine learning algorithm, a 10-fold cross-validation method is used. For deep learning algorithm, an Adam

optimiser with a fixed learning rate of 0.001 was used. To prevent it from the overfitting problem, both dropout and early stopping approaches were employed.

The error rate and accuracy are measured as shown in Equations (8) and (9). We take the error rate of each solution as the fitness value. Note that all the error rates shown in this paper are the average value of the validation over 10 folds, and with this setting a solution, a lower fitness value is a better solution.

$$Err = \frac{False\ Positive + False\ Negative}{Total\ number\ of\ data} \quad (8)$$

$$Accuracy = 1 - Err \quad (9)$$

2.6 | Optimisation problem formulation and challenges

The 10-fold classification error rate $P_x(t)$ serves as the minimisation objective. Mathematically, the minimisation problem can be expressed as Equation (10),

$$\min_x P_x(t) \quad (10)$$

where x is a set of parameters in the HAR system that defines the system and t is the validation sample, which is randomly chosen for every function evaluation.

At the optimisation stage, there are 12 parameters in total. They are divided into two groups according to whether they are continuous or not.

The first group parameter is discrete, including 'Window', 'Mask', 'Masked phase', 'Masked unwrapped phase', 'Spectrogram', 'Masked spectrogram (patent)', and 'Masked spectrogram (radar)'. They have two options: 0 and 1. For 'Window', 0 means rectangular window and 1 means Hamming window. For other six parameters, 0 means combination excludes it, and 1 means combination that includes it.

The second group parameter is continuous, including overlapping factor F (ranging from 0.5 to 0.95), time window length W (ranging from 100 to 1000), V (ranging from 0.01 to 1) and T_e (ranging from −20 to 20) in the thresholding method, and clipping time K (ranging from 1.5 to 5s). Note that T_e has to be integer and other parameter can be any value in the range.

Parametric sweeping is a widely used method to find the set of parameters x to optimise the classification accuracy. However, this method only works for small-scale problems due to its large computing overhead. For the targeted 12-dimensional problem with wide search ranges, where each function evaluation costs 3 min in our workstation, the computing overhead is still unaffordable even using modern intelligent optimisation techniques, for example, DE algorithm [29], genetic algorithm [36], and particle swarm optimisation [30]. Hence, obtaining optimal global solutions efficiently becomes the central challenge.

2.7 | The SADEA algorithm and parameter settings

To the best of our knowledge, there are few off-the-shelf methods to address the above challenge in the signal processing field. The SADEA-I [37, 38], usually applied to antenna design optimisation, is adapted for HAR. Surrogate model-assisted differential evolutionary algorithm can obtain comparable optimisation ability with the DE algorithm, which shows excellent optimisation ability, while reducing by a factor 5–10 the necessary number of function evaluations compared to using the standard DE [13]. The flowchart of SADEA-I is illustrated in Figure 3. The adapted SADEA-I algorithm for HAR is summarised as follows.

- Step 1: Latin Hypercube Sampling is applied to generate *NP* samples to form an initial database with *NP* exact function evaluations.
- Step 2: The classification error rate is minimised until a suitable x with the lowest classification error rate among those in the database satisfy the preset error rate threshold or the total optimisation time exceeds the preset threshold.
- Step 3: Obtain λ best sets of solutions as the parent population to form a child population by applying the DE mutation and crossover operations [29].
- Step 4: For each child solution, obtain its training data by collecting their nearest τ known samples from the database and train Gaussian Process (GP) models [39]. Predict classification error rate and uncertainty for each child solution.
- Step 5: Prescreen the child population with the predicted values and prediction uncertainty using the lower confidence bound (LCB) method [40, 41] and obtain the estimated most promising candidate solution. Carry out an exact function
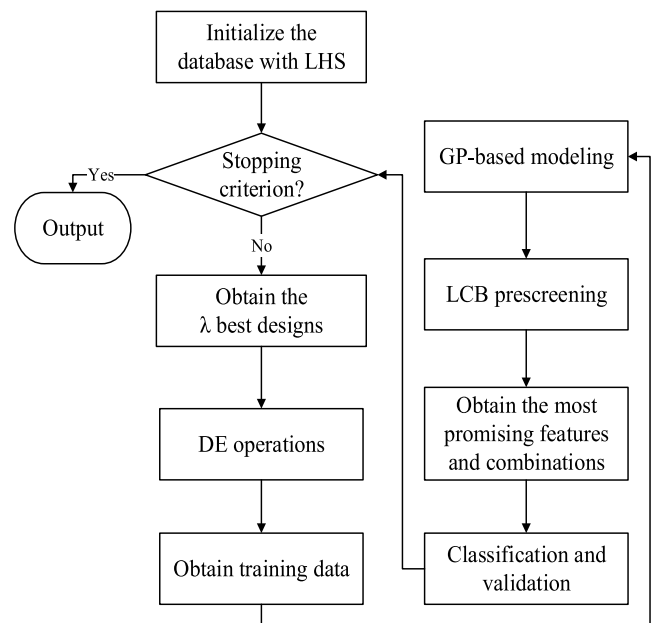

FIGURE 3 Hierarchical structure of the solution algorithm.

evaluation for it. The candidate solution and its function value are appended to the database and go back to Step 2.

In this case, Gaussian Process models are trained to predict and suggest the most promising candidate parameter set in each iteration. Hence, it significantly reduces the number of exact function evaluations needed for the search. To make GP and DE work harmoniously, the surrogate model-aware evolutionary framework is used and more details can be found in [42].

The algorithm parameters are set following [37, 43]: NP is set to be 50. Both mutation rate and crossover rate are set to be 0.8. λ is set to be the same as NP. The number of training samples τ is also set to be 50 to train GP models. In LCB prescreening, ω is set to be 2.

3 | RESULTS AND DISCUSSION

The entire AI-driven holistic HAR system optimisation was implemented using a workstation with an AMD Ryzen 9 3900X 12-core processor (3.8 GHz) and an NVIDIA GeForce GT 710 GPU. In this study, binary parameters are treated as continuous variables with values from 0 to 1 and rounded off to the nearest integers. A reference design was based on our previous experiment [28], produced by the adaptive thresholding method with parameter sweeping on adaptive thresholding T_e and feature fusion of six domains. The reference performance in this experiment is based on the human operator that achieved the classification error rate—manually tuned results—[13], which is based on the operator's domain knowledge.

3.1 | Support vector machine classifiers with adaptive thresholding for surrogate model-assisted differential evolutionary algorithm

The optimisation convergence trend is shown in Figure 4. The red dotted line represents the manual design result, where the error rate is 21.98%. After 2000 function evaluations using SADEA-I, the system is optimised and achieves an error rate from 16.50% to 10.59% in three independent optimisation runs. Compared to the manually tuned reference system, the holistic approach decreases the error rate by 5.48%–11.39%.

Table 5 illustrates the details of the optimal parameters and combinations when the optimisation algorithm converges. The result shows that for our human activity dataset, the error rate reaches the minimum with the highest overlapping factor and minimum time window length. In addition, the clipping time is 4.58 s and the adaptive thresholding parameters V and T_e are 0.9166 and 3, respectively. These values were in line with the general trend found in a parametric sweeping on the different domains, which identified T_e to be optimal between 0 and 5 of the adaptive threshold value for $V = 0.1$ [11]. The effectiveness and necessity of research on thresholding are demonstrated in an improvement of ~11% using the SADEA-I method in only 2000 function evaluations (3 min per evaluation). All MDS representations were selected but Domain 1. Domain 1
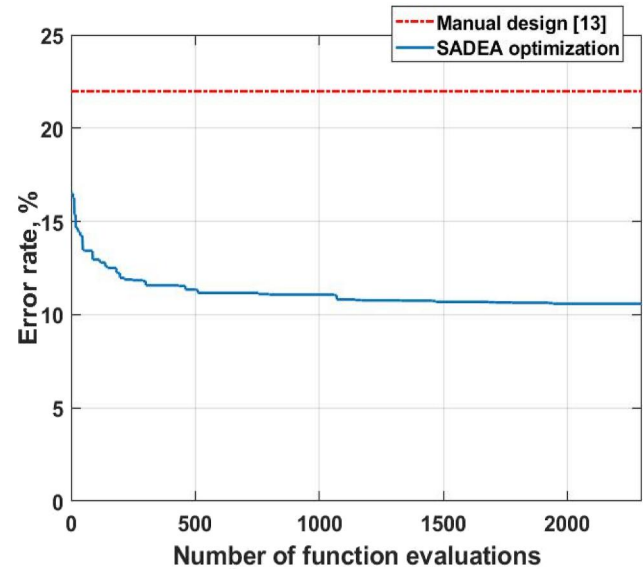

FIGURE 4 Convergence trend of surrogate model-assisted differential evolutionary algorithm (SADEA-I) with support vector machine classifiers (SVM) and comparison with manual design results.

TABLE 5 Tuned parameters and selected domains.

Time window length	Overlapping factor	Clipping time	Difference value V
154 ms	0.95	4.58s	0.9166

Adaptive thresholding Type	FFT window type	Selected domains of radar
3	Hamming	Domains 2–6

(Unfiltered MDS Amplitude) is excluded from the most suitable combination, which identifies that the "raw" spectrogram is not optimal and the research on adaptive thresholding and its application in different MDS representations is essential as they all contain salient information for classification although more difficult to interpret visually.

3.2 | AlexNet with adaptive thresholding for surrogate model-assisted differential evolutionary algorithm

For this experiment, the dataset was partitioned into three subsets: training, validation, and testing, with a ratio of 7:2:1, respectively. The performance of our experiment is evaluated on the basis of the testing set results. In alignment with the previous 10-fold cross validation results, we also carry out this experiment 10 times, considering the mean accuracy of iterations as our final performance of the algorithm.

Figure 5 demonstrates the optimisation convergence trend of SADEA-I with AlexNet. It also presents the result of manual design parameters on AlexNet. When combined with AlexNet, the SADEA-I is optimised in 700 function

evaluations, with averaged error rate decreased from 17.83% to 6.46%. Compared with manual design result with an error rate of 9.14%, the holistic approach can yield a worse result with an extra 8.69% error rate or decreased error rate by 2.68%.

Table 6 illustrates the details of convergence trend along with the optimal parameters and combinations realised at the point of convergence of the optimisation algorithm. The result is slightly different from the previous findings. The Hamming window continues to present the most effective option, yielding superior accuracy. The time window length has escalated to 390 ms. The adaptive thresholding parameters, V and T_e, are determined to be 0.8249 and −13, respectively. The V changes to a minor but close value, while T_e has exhibited significant alteration. This result indicates the success of our adaptive thresholding algorithm.

3.3 | Discussions

Compared with SADEA-I and SVM results, SADEA-1 with AlexNet achieves further improvement of approximately 5% over merely 700 function evaluations, which reduces more than half of evaluations to convergence. All radar representations were chosen, including domain I, which highlights the enhanced
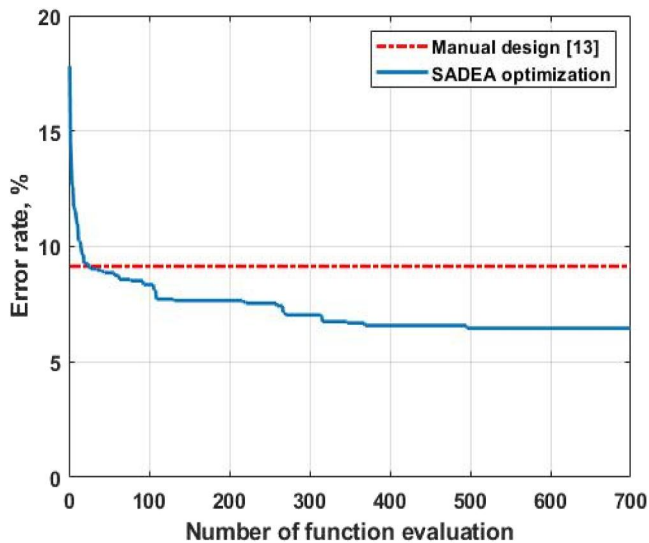

FIGURE 5 Convergence trend of surrogate model-assisted differential evolutionary algorithm (SADEA-I) with AlexNet and comparison with manual design results.

interpretative capability provided by the AlexNet model. However, there is a significant change observed in the length of the time window. This variance could potentially be attributed to the influence of a higher frequency resolution, which results in a more intricate graphical representation of the data. The finer resolution provides an enriched data for the automatic extraction of features within the deep learning model, thereby augmenting its ability to identify distinctive patterns.

Table 7 concludes the comparison of statistics of SADEA algorithms paired with different classifiers. For SADEA-I with SVM, the optimised error rate decreases from 16.50% to 10.59% with 2000 function evaluations, compared to 21.98% from a human operator. This means that SADEA-I with SVM can boost the performance of our classification by 5.48%–11.39% in 4 days compared to 3 months of manual tuning by the human operator. The second method SADEA-I with AlexNet exhibits an error rate reduction from 17.83% to 6.46% with 700 function evaluations compared to 9.14% from a human operator. We observe that the error rate with SADEA-I with AlexNet can reach a minimum error rate of 6.46%, which is 4.13% better than SADEA-I with SVM. However, the maximum error of SAEDEA-I with SVM is 1.33% better than SADEA-I with AlexNet. These statistics indicate the efficacy of the SADEA-I algorithm when interfaced with various classifiers. Deep learning models tend to be more computationally intensive, but with SADEA, it appears that the number of function evaluations are drastically reduced by 2.85 times in this case. This suggests that the SADEA algorithm boosts convergence towards optimal solutions more efficiently when combined with the deep learning algorithm, thus leading to potentially improved performance with fewer evaluations. However, note that the error rate for SADEA-I with AlexNet is more volatile (11.37%) than with SVM (5.91%). Moreover, SADEA-I with SVM did not incorporate feature selection to enhance performance at this stage. Feature selection can reduce the overall complexity and improve the performance when combined with the adaptive thresholding method [34]. As we continue to refine our holistic techniques, feature selection will be included for our future plan; however, SADEA-I could not handle these many variables to tune at once. The next version of SADEA will be able to handle more tuning parameters for further optimisation. We also compare our results with different models using the same dataset [5] to illustrate the potential improvements with our proposed method. Table 8 shows that our methods can achieve good accuracy with computationally light classification algorithms and reach performances compared to deeper implementations.

TABLE 6 Tuned parameters and selected domains.

Time window length	Overlapping factor	Clipping time	Difference value V
390 ms	0.87	5 s	0.8249
Adaptive thresholding Type	**FFT window type**	**Selected domains of radar**	
−13	Hamming	Domains 1–5	

TABLE 7 Statistics of the best function values obtained by SADEA with different classifiers.

Method	Best error rate (%)	Worst error rate (%)	Human error rate (%)	Function evaluations
SADEA-I with SVM	10.59	16.50	21.98	2000
SADEA-I with AlexNet	6.46	17.83	9.14	700

Abbreviation: SADEA, surrogate-model-assisted differential evolution algorithm.

This shows that our holistic approach could improve further these architectures for HAR to optimise accuracy.

4 | CONCLUSION

In this study, SADEA-I has been applied for the efficient holistic optimisation of parameter tuning for signal data pre-processing, the radar representation selection, our patented adaptive thresholding methods, and classifiers. We assessed the performance of the holistic approach on the joint tuning of signal processing, adaptive thresholding and classification for two distinct classification models. The SVM classifier achieves an accuracy up to 89.41% after 2000 function evaluations and the AlexNet achieves an accuracy up to 93.54% after ~700 function evaluations. Notably, both classifiers displayed superior performance when contrasted with their counterparts that lacked SADEA-I algorithm. The accuracies can be improved by 11.30% and 2.68%, respectively. It also illustrates its strength on time-efficiency attributes. The results, which would conventionally require months for parametric sweeping by a human operator, are accomplished by SADEA-I within a span of 84 h.

This proof-of-concept (POC) experiment on SADEA-I encompasses the whole FFT-based signal processing chain and the many representations of MDS. This POC is crucial as we mentioned many more data representation domains that can be fused for classification and optimising performances with increasing dimensionality. Furthermore, the explosion of civilian and military applications with MIMO radar and 6G sensing will further increase dimensionality with multiple channels that are all processed using a generic pre-processing chain and not tuned individually.

Building on this proof-of-concept, the model is being refined to be incorporated as an optimiser to allow other researchers to try it on their algorithms and data. We also intend to expand this research to wider time-frequency transforms with SADEA-I to further optimise the accuracy and to add objective functions to consider the computational efficiency of the different stages. In addition, this parametric search can be extended to deep learning model. For instance, parameters, such as the learning rate, which play a crucial role in how quickly or slowly a model learns, can be optimised using similar methods. By leveraging the method of parametric search, we can systematically explore different parameters and select an optimal value that allows for effective learning within a reasonable amount of time.

Furthermore, as radar costs are going down, we should tackle the remaining open challenges of target aspect angle robustness in classification and fusion with other sensing modalities to compensate with the shortcomings of individual sensors. Radar is promising in the field of assisted living, but challenges remain in terms of blind regions, obstruction in the radar path and mutual interference when several radar systems operate in the same vicinity.

ORCID
Zhenghui Li https://orcid.org/0000-0003-0170-4686
Julien Le Kernec https://orcid.org/0000-0003-2124-6803

TABLE 8 Performance comparison between the proposed method and alternative methods.

Model	Accuracy (%)
VGG 19 [44]	93
MobileNetV2 [45]	95.43
Alexnet [46]	89
VGG19 pruning 0.7 [44]	94
Double CNNs [47]	94.8
Manuel optimisation SVM + feature selection [34]	92.2
SADEA-I with SVM	89.41
SADEA-I with AlexNet	93.54

Abbreviations: CNN, convolutional neural network; SADEA, surrogate-model-assisted differential evolution algorithm.

REFERENCES
1. Le Kernec, J., et al.: Radar signal processing for sensing in assisted living: the challenges associated with real-time implementation of emerging algorithms. IEEE Signal Process. Mag. 36(4), 29–41 (2019)
2. Palipana, S., et al.: FallDeFi. Proc. ACM Interact Mob Wearable Ubiquitous Technol. 1(4), 1–25 (2018). https://doi.org/10.1145/3161183
3. Amin, M.G., et al.: Radar signal processing for elderly fall detection: the future for in-home monitoring. IEEE Signal Process. Mag. 33(2), 71–80 (2016). https://doi.org/10.1109/msp.2015.2502784
4. Gurbuz, S.Z., Amin, M.G.: Radar-based human-motion recognition with deep learning: promising applications for indoor monitoring. IEEE Signal Process. Mag. 36(4), 16–28 (2019). https://doi.org/10.1109/msp.2018.2890128
5. Yang, S., et al.: The human activity radar challenge: benchmarking based on the 'radar signatures of human activities' dataset from Glasgow University. IEEE J. Biomed. Heal. Inform. 27(4), 1813–1824 (2023). https://doi.org/10.1109/jbhi.2023.3240895

6. Chen, V.C., et al.: Micro-Doppler effect in radar: phenomenon, model, and simulation study. IEEE Trans. Aerosp. Electron. Syst. 42(1), 2–21 (2006). https://doi.org/10.1109/taes.2006.1603402

7. Li, X., He, Y., Jing, X.: A survey of deep learning-based human activity recognition in radar. Rem. Sens. 11(9), 1068 (2019). https://doi.org/10.3390/rs11091068

8. Du, Y., et al.: Radar-based human activity classification with cyclostationarity. In: 2021 CIE International Conference on Radar (CIE Radar 2021) (2021)

9. Zhou, B., et al.: Simulation framework for activity recognition and benchmarking in different radar geometries. IET Radar, Sonar Navig. 15(4), 390–401 (2021). https://doi.org/10.1049/rsn2.12049

10. Palipana, S., et al.: Pantomime: mid-air gesture recognition with sparse millimeter-wave radar point clouds. Proc. ACM Interact Mob Wearable Ubiquitous Technol. 5(1), 1–27 (2021). https://doi.org/10.1145/3448110

11. Bhavanasi, G., et al.: Patient activity recognition using radar sensors and machine learning. Neural Comput. Appl. 34(18), 16033–16048 (2022). https://doi.org/10.1007/s00521-022-07229-x

12. Zhu, J., Chen, H., Ye, W.: A hybrid CNN–LSTM network for the classification of human activities based on micro-Doppler radar. IEEE Access 8, 24713–24720 (2020). https://doi.org/10.1109/access.2020.2971064

13. Zhang, R., Cao, S.: Real-time human motion behavior detection via CNN using mmWave radar. IEEE Sens. Lett. 3(2), 1–4 (2019). https://doi.org/10.1109/lsens.2018.2889060

14. Singh, A.D., et al.: RadHAR. In: Proceedings of the 3rd ACM Workshop on Millimeter-Wave Networks and Sensing Systems, pp. 51–56 (2019)

15. Li, X., et al.: Hierarchical radar data analysis for activity and personnel recognition. Rem. Sens. 12(14), 2237 (2020). https://doi.org/10.3390/rs12142237

16. Loukas, C., et al.: Activity classification using raw range and I & Q radar data with long short term memory layers. In: 2018 IEEE 16th Intl Conf on Dependable, Autonomic and Secure Computing, 16th Intl Conf on Pervasive Intelligence and Computing, 4th Intl Conf on Big Data Intelligence and Computing and Cyber Science and Technology Congress (DASC/PiCom/DataCom/CyberSciTech), pp. 441–445 (2018)

17. Jokanovic, B., Amin, M., Erol, B.: Multiple joint-variable domains recognition of human motion. In: 2017 IEEE Radar Conference (RadarConf), pp. 0948–0952 (2017)

18. Li, Y., et al.: Potential active shooter detection based on radar micro-Doppler and range-Doppler analysis using artificial neural network. IEEE Sensor. J. 19(3), 1052–1063 (2019). https://doi.org/10.1109/jsen.2018.2879223

19. Erol, B., Amin, M.G.: Radar data cube processing for human activity recognition using multisubspace learning. IEEE Trans. Aerosp. Electron. Syst. 55(6), 3617–3628 (2019). https://doi.org/10.1109/taes.2019.2910980

20. Li, H., et al.: Bi-LSTM network for multimodal continuous human activity recognition and fall detection. IEEE Sensor. J. 20(3), 1191–1201 (2020). https://doi.org/10.1109/jsen.2019.2946095

21. Ding, C., et al.: Fall detection with multi-domain features by a portable FMCW radar. In: 2019 IEEE MTT-S International Wireless Symposium (IWS), pp. 1–3 (2019)

22. Guo, J., et al.: Complex field-based fusion network for human activities classification with radar. In: IET International Radar Conference (IET IRC 2020), pp. 68–73 (2021)

23. Meng, Z., et al.: Gait recognition for Co-existing multiple people using millimeter Wave sensing. Proc. AAAI Conf. Artif. Intell. 34(01), 849–856 (2020). https://doi.org/10.1609/aaai.v34i01.5430

24. Rahman, M.M., Gurbuz, S.Z., Amin, M.G.: Physics-aware design of multi-branch GAN for human RF micro-Doppler signature synthesis. In: 2021 IEEE Radar Conference (RadarConf21), pp. 1–6 (2021)

25. Yang, Z., et al.: Real-time human activity classification from radar with CNN-LSTM network. In: 2021 IEEE 16th Conference on Industrial Electronics and Applications (ICIEA), pp. 50–55 (2021)

26. Centre National de la Recherche Scientifique: Device for Characterizing the Actimetry of a Subject in Real Time. WO2021069518A1 (2021)

27. Centre National de la Recherche Scientifique: Method and Device for Human Activity Classification Using Radar Micro Doppler and Phase, pp. EP21306742 (2022)

28. Li, Z., et al.: Human activity classification with adaptive thresholding using radar micro-Doppler. In: 2021 CIE International Conference on Radar (CIE Radar 2021) (2021)

29. Storn, R., Price, K.: Differential evolution--a simple and efficient heuristic for global optimization over continuous spaces. J. Global Optim. 11(4), 341–359 (1997). https://doi.org/10.1023/a:1008202821328

30. Kennedy, J., Eberhart, R.: Particle swarm optimization. In: Proceedings of ICNN'95-international Conference on Neural Networks, vol. 4, pp. 1942–1948 (1995)

31. Fioranelli, F., et al.: Radar sensing for healthcare. Electron. Lett. 55(19), 1022–1024 (2019). https://doi.org/10.1049/el.2019.2378

32. Fioranelli, F., et al.: Radar Signatures of Human Activities. [Data Collection] (2019). [Online]. https://researchdata.gla.ac.uk/848/

33. Fioranelli, F., et al.: Radar-based evaluation of lameness detection in ruminants: preliminary results. In: IEEE MTT-S 2019 International Microwave Biomedical Conference, IMBioC 2019 - Proceedings, vol. 1, pp. 1–4 (2019)

34. Li, Z., et al.: Radar-based human activity recognition with adaptive thresholding towards resource constrained platforms. Sci. Rep. 13(1), 3473 (2023). https://doi.org/10.1038/s41598-023-30631-x

35. Krizhevsky, A., Sutskever, I., Hinton, G.E.: ImageNet classification with deep convolutional neural networks. Commun. ACM 60(6), 84–90 (2017). https://doi.org/10.1145/3065386

36. Whitley, D.: A genetic algorithm tutorial. Stat. Comput. 4(2), 65–85 (1994). https://doi.org/10.1007/bf00175354

37. Liu, B., et al.: An efficient method for antenna design optimization based on evolutionary computation and machine learning techniques. IEEE Trans. Antenn. Propag. 62(1), 7–18 (2013). https://doi.org/10.1109/tap.2013.2283605

38. Liu, B., Koziel, S., Ali, N.: SADEA-II: a generalized method for efficient global optimization of antenna design. J. Comput. Des. Eng. 4(2), 86–97 (2017). https://doi.org/10.1016/j.jcde.2016.11.002

39. Santner, T.J., et al.: The Design and Analysis of Computer Experiments, vol. 1. Springer (2003)

40. Dennis, J.E., Torczon, V.: Managing approximation models in optimization. Multidiscip. Des. Optim. State-of-the-Art 5, 330–347 (1997)

41. Emmerich, M.T.M., Giannakoglou, K.C., Naujoks, B.: Single-and multiobjective evolutionary optimization assisted by Gaussian random field metamodels. IEEE Trans. Evol. Comput. 10(4), 421–439 (2006). https://doi.org/10.1109/tevc.2005.859463

42. Liu, B., Zhang, Q., Gielen, G.G.E.: A Gaussian process surrogate model assisted evolutionary algorithm for medium scale expensive optimization problems. IEEE Trans. Evol. Comput. 18(2), 180–192 (2013). https://doi.org/10.1109/tevc.2013.2248012

43. Akinsolu, M.O., et al.: A parallel surrogate model assisted evolutionary algorithm for electromagnetic design optimization. IEEE Trans. Emerg. Top. Comput. Intell. 3(2), 93–105 (2019). https://doi.org/10.1109/tetci.2018.2864747

44. Hao, D., et al.: A compact human activity classification model based on transfer learned network pruning. In: IET International Radar Conference (IET IRC 2020), pp. 1488–1492 (2021)

45. Xiaolong, Z., Tian, J., Hao, D.: A lightweight network model for human activity classifiction based on pre-trained mobilenetv2. In: IET International Radar Conference (IET IRC 2020), pp. 1483–1487 (2021)

46. Kim, Y., Moon, T.: Human detection and activity classification based on micro-Doppler signatures using deep convolutional neural networks. IEEE Geosci. Remote Sens. Lett. 13(1), 8–12 (2016). https://doi.org/10.1109/lgrs.2015.2491329

47. Chen, Z., Li, G.: Human activity classification with neural network using radar micro-Doppler and range signatures. In: IET International Radar Conference (IET IRC 2020), pp. 222–227 (2021)